

Gravitational Waves from Extragalactic Inspiring Binaries: Selection Effects and Expected Detection Rates

Philip Nutzman¹, Vicky Kalogera¹, Lee Samuel Finn²,
Cy Hendrickson¹, Krzysztof Belczynski^{1,3}

¹*Northwestern University, Dept. of Physics & Astronomy, 2145 Sheridan Rd., Evanston,
IL 60208*

²*Center for Gravitational Wave Physics, The Pennsylvania State University, University
Park, PA 16802*

³*Lindheimer Postdoctoral Fellow
me, vicky, c-hendrickson, belczynski@northwestern.edu; and LSFinn@PSU.Edu*

ABSTRACT

We examine the selection effects that determine how the population of inspiraling binary compact objects (BCOs) is reflected by those potentially observed with ground-based interferometers like LIGO. We lay the ground-work for the interpretation of future observations in terms of constraints on the real population and, correspondingly, binary star evolution models.

To determine the extra-galactic population of inspiraling binaries we combine data on distance and blue luminosity from galaxy catalogs with current models of the galactic BCO mass distribution to simulate the physical distribution of binaries in the nearby universe. We use Monte Carlo methods to determine the fraction of binaries observable by the LIGO detectors from each galaxy as a function of the BCO chirp mass. We examine separately the role of source distance, sky position, time of detection, and binary system chirp mass on detection efficiency and selection effects relevant to the three LIGO detectors. Finally, we discuss the implications of the nearby geography of space on anticipated GW detection and compare our results to previous studies, which have assumed uniform galaxy volume density and fixed chirp mass for binary compact objects.

From these considerations, actual BCO inspiral observations or significant upper limits on the coalescence rate anticipated in the near future by ground-based interferometers can be used to improve our knowledge of the galactic binary inspiral rate and to constrain models of radio pulsar characteristics and binary star evolution channels leading to neutron star or black hole binaries.

Subject headings: binaries: close—gravitational waves—stars: neutron, black hole

1. Introduction

Binary compact objects (BCO) with neutron stars or black holes hold a special place among gravitational wave (GW) sources. The discovery of PSR B1913+16 (Hulse & Taylor 1974), the first binary pulsar system, inspired the detailed study of inspiraling compact binaries and provided the first observational evidence for the existence of gravitational radiation (Taylor & Weisberg 1989). Binary systems like PSR B1913+16 are driven to coalescence by a GW emission catastrophe: in the last approximately 20 s before they coalesce they radiate their remaining binding energy (approximately 2×10^{52} ergs) as gravitational waves in a band accessible to the large ground-based detectors like the Laser Interferometer Gravitational Wave Observatory (LIGO; Abbott et al. 2003a) and VIRGO (Caron et al. 1997)¹.

Current observational constraints on the population of neutron star or black hole binary systems depend on radio pulsar observations of just a handful of Galactic binary systems (e.g., Burgay et al. 2003; Kalogera et al. 2003). In contrast, the LIGO and VIRGO detectors will observe stellar mass inspiraling BCOs at extra-galactic distances. They will also be sensitive to black hole binaries, which are not observable electromagnetically. Correspondingly, observations by this new generation of detectors can help constrain the binary coalescence rate density in the nearby Universe, and binary evolution models for the formation of such sources, in ways not possible with electromagnetic observations alone. In this work we begin laying the ground-work for the astrophysical interpretation of future GW observations of BCO inspiral by focusing attention on the selection effects associated with GW observations: in particular, effects associated with binary component masses, the GW antenna beam and the local geography of the Universe.

Over the past decade there have been many predictions of the detection rate in LIGO of BCO inspirals (e.g., Belczynski, Kalogera, & Bulik 2002; Kalogera et al. 2003). These calculations all begin by estimating the Galactic coalescence rates and extrapolating it to other galaxies. The observed rate is then calculated assuming that galaxies (and, thus, binaries) are distributed homogeneously and isotropically in the local universe, and that the LIGO detector observes all coalescing binaries inside a fixed distance, which is the radius of a sphere that would have the same volume as is effectively surveyed by the detector. These approximations are inadequate when we wish to go beyond order-of-magnitude predictions and actually interpret observed events as constraints on the actual compact object binary

¹Somewhat less energy will be radiated in the bands accessible GEO (Abbott et al. 2003a) and TAMA (Ando et al. 2001), and less still in the bands accessible to the bar detectors AURIGA (Prodi et al. 1998), ALLEGRO (Mauceli et al. 1996), EXPLORER (Astone et al. 1993; Amaldi et al. 1986) and NAUTILUS (Astone et al. 1997).

population, as is our goal.

To improve on past models for the physical population of inspiraling compact binary systems, we use galaxy catalogs to model the actual distribution of galaxies in the local universe and we use stellar synthesis calculations (specifically those of Belczynski, Kalogera, & Bulik 2002) to model the mass distribution of binaries within each galaxy. From the constructed population models, we determine the compact binary coalescence rate and distribution with binary system mass that we expect the LIGO detector system to observe, taking full account of each galaxy’s distance and declination, the LIGO detector system’s noise spectrum, and its position and orientation on Earth.

Our principal goal in relating a physical population model to the distribution that we expect modern GW detectors to observe is to enable observations by those detectors to constrain the population model (see Bulik & Belczynski 2003 and Bulik, Belczynski, & Rudak 2004 for recent studies with similar goals). Through the calculations described here, comparison of future observed rates or rate upper limits constrain stellar synthesis models and the overall binary compact object population. While our principal interest is in preparing for this kind of interpretation of forthcoming observations, as a by-product of our investigations we have improved detection rate predictions as well.

In §2 we present an overview of the various approaches used so far for the extrapolation of Galactic detection rates to extragalactic distances and introduce our novel galaxy-by-galaxy approach, whereby we calculate the detectability of BCO inspiral for each galaxy in our catalog. In §3 we describe how we calculate, from the detailed extra-galactic population model described in §2, the observed distribution of BCOs. In §4 we discuss our results, including the LIGO detector system’s efficiency for detecting binaries from different galaxies in the nearby universe, the expected observed coalescing binary mass distribution, new detection rate predictions, and the implications of the geography of the nearby universe for detection of binary compact object systems. We end in §5 with a summary of our main conclusions.

2. Estimating the Binary Compact Object Population Density in the Nearby Universe

Our final goal is to understand how the actual population and distribution of coalescing binary compact objects (BCOs) is mapped to GW observations by LIGO (or GEO, TAMA or VIRGO) of inspiraling binary systems. The signal amplitude depends on the system’s distance, location on the detector’s sky, orbital plane inclination with respect to the detector

line-of-sight, and the binary chirp mass (cf. eq.[4b]). In this section we characterize the compact object binary population distribution in space and component masses: i.e., the density as a function of distance, position on the detector sky, and the chirp mass.

2.1. Previous Studies

All studies of compact object coalescence GW detection rates begin with an estimate of the intrinsic coalescence in our own Galaxy. Two methods have been employed to derive these rates: statistical analysis of the observed sample of inspiral binary candidates and theoretical investigations based on understanding of BCO formation. The first approach so far provides us with the best rate constraints (see Burgay et al. (2003) and Kalogera et al. (2003) for the most recent estimates in view of a newly discovered NS-NS system), but is still limited by a small observed sample (currently 3 systems), some uncertainty in the selection effects associated with, e.g., pulsar beaming and radio luminosity, and by the absence of known BH-NS and BH-BH binaries. The second approach provides us with results for all types of BCOs based on binary population synthesis models, which are generally calibrated to match the empirical estimates of Type II supernova rates (Belczynski, Kalogera, & Bulik 2002, hereafter BKB and references therein), but the uncertainties associated with binary evolution models are significant. At present our best estimates of Galactic coalescence rates place them in the range of $10^{-5} - 10^{-3} \text{ yr}^{-1}$ for NS-NS, $10^{-6} - 10^{-4} \text{ yr}^{-1}$ for BH-NS, and $0 - 10^{-4} \text{ yr}^{-1}$ for BH-BH.

All extrapolations from Galactic rates to extragalactic rates are based on the assumption that the formation of BCOs in a region is proportional to the blue luminosity in that region, corrected for reddening (Phinney 1991). Correspondingly, the coalescence rate density R_{det} within a distance D_{max} is proportional to the Milky Way coalescence rate density R_{MW} and the ratio of the blue luminosity within the sphere to the Milky Way blue luminosity:

$$R_{\text{det}} = \left(\frac{\mathcal{L}_b}{L_{\text{MW}}} \right) \left(\frac{4}{3} \pi D_{\text{max}}^3 \right) R_{\text{MW}}, \quad (1)$$

where \mathcal{L}_b is the mean blue luminosity volume density within a distance D_{max} , L_{MW} is the total blue luminosity of the Milky Way, and R_{MW} is the coalescence rate in the Milky Way. The distance D_{max} is calculated so that, if coalescing binaries with given component masses (e.g., $1.4 M_{\odot}$) are assumed to be uniformly distributed throughout space with rate density \dot{n} , the rate of detections in a GW detector above a given signal-to-noise ratio is

$$\dot{N}_{\text{GW}} = \frac{4\pi}{3} D_{\text{max}}^3 \dot{n}; \quad (2)$$

i.e., D_{\max} is the radius of a sphere whose volume is the effective volume surveyed by the detector for binary systems with these component masses (Finn 1996, 2001a; Kalogera et al. 2001).

2.2. A Galaxy Catalog Approach

Here we describe a method appropriate for extrapolating Galactic BCO coalescence rates beyond the galaxy, for the purpose of estimating inspiral detection rates in GW detectors. Our ultimate goal is not the prediction of what might be seen, but to understand how observed bounds on the coalescence rate, perhaps as a function of the BCO component masses determined from these observations, can inform our understanding of binary populations in galaxies and binary population synthesis. Toward that end we improve on the method of binary inspiral rate estimation, described in section 2.1, in three ways:

1. The blue luminosity scaling argument is accurate when the survey volume is so large that local fluctuations in the galaxy density and the blue luminosity per galaxy are small. This is not the case in the local universe, where the galaxy distribution is strongly anisotropic. To overcome this difficulty we make use of galaxy catalogs to map the true distribution of galaxies in space and in blue luminosity.
2. The LIGO detectors sensitivity is not isotropic: e.g., it is more sensitive to binaries immediately above and below the plane of the detectors arms than to binaries in the detector plane. We take full account of the detector’s actual beam and its orientation with respect to the sky, averaged over the sidereal day.
3. Estimates to date use a D_{\max} chosen for a particular combination of component masses.² We estimate the inspiral detection rate for the theoretically expected distribution of component masses, as opposed to some canonical mass.

2.2.1. Spatial Distribution of Galaxies

Galaxies are distributed anisotropically in the local universe, and this affects the interpretation of BCO inspiral detection rates in terms of galactic populations of BCOs. To take into account the nearby distribution of galaxies, we draw galaxy data from two catalogs: the

²In previous surveys binaries are assumed to be either double neutron star, with component masses of $1.4 M_{\odot}$, or black hole neutron star binaries, with component masses of $10 M_{\odot}$ and $1.4 M_{\odot}$.

Lyon-Meudon extragalactic database (Paturel et al. 1989, hereafter LEDA), and the Tully Nearby Galaxy Catalog (Tully 1988, hereafter NBG).³ We select these galaxy data sources for their homogeneous coverage of the sky: GW detectors have some sensitivity to BCOs in every direction on the sky and so data from surveys that cover only sectors of the sky, such as the Sloan Digital Sky Survey (York et al. 2000), are not adequate.

Our principal source of galaxy data is the LEDA. It is comprehensive for galaxies with blue magnitudes brighter than 14.5 and partially complete for those as faint as $m = 17$ (Paturel et al. 1989). Owing to the difficulties in determining galaxy distances, LEDA lacks distance data for all but a small fraction of its galaxies. The NBG, on the other hand, has excellent information for galaxies with radial velocity less than 2500 km/s, but makes no attempt to be comprehensive beyond that range (Tully 1988). In order to have available the best galactic distance estimates we use the NBG distance data with the corresponding LEDA galaxies and derive distances for all other LEDA galaxies using the measured radial velocities and $H_0 = 70 \text{ km s}^{-1} \text{ Mpc}^{-1}$. Our synthesized catalog thus provides the needed parameters of right ascension α , declination δ , distance D , and blue luminosity corrected for reddening for each galaxy.

A primary concern with any galaxy catalog is incomplete coverage of faint galaxies. Our catalog is complete for galaxies brighter than blue magnitudes 14.5; correspondingly, incompleteness is important for faint galaxies beyond approximately 20 Mpc and for galaxies of increasing intrinsic brightness at greater distances.

To compensate for the missing galaxies while still accounting for their non-uniform spatial distribution we introduce a distance-dependent correction factor, which is the ratio of the expected blue luminosity, were the catalog is complete, to the blue luminosity reported by the catalog at each distance. To derive this factor we calculate the expected distribution of luminosity with distance assuming that the true distribution with distance is proportional to the luminosity distribution at that distance for galaxies *brighter* than the completeness at each distance. Since our galaxy catalog is essentially complete with regards to cumulative blue luminosity up to approximately 22 Mpc, we calibrate the resulting distribution to match the catalogued distribution at this distance.

³Previous work by Lipunov et al. (1995) similarly utilizes the Tully Nearby Galaxy Catalog to map the distribution of gravitational wave sources. Note that our purpose and analysis greatly diverges from this earlier work; our emphasis on selection effects demands different considerations (e.g., knowledge of detector location, orientation and noise characteristics, correct compensation for incompleteness of galaxies in Tully’s NBG and galaxies beyond the range of NBG, etc) and enables us to consider different questions from those in Lipunov et al.

Figure 1 shows the corrected cumulative blue luminosity as a function of distance. For comparison we show also the cumulative blue luminosity expected under the assumption of uniform blue luminosity density as adopted in Kalogera et al. (2001). The normalization of the uniform density blue luminosity curve is based on galaxy surveys out to large distances. Three elements of this figure are worth noting in more detail. First, the uniform blue luminosity density approximation clearly underestimates the actual blue luminosity contributed by nearby galaxies. Second, the Virgo cluster contributes to a large step in the cumulative blue luminosity at approximately 20 Mpc. The higher local blue luminosity density at this distance significantly increases the estimated detection rate as a fraction of the total number of coalescing systems, especially for initial detectors. Finally, beyond the Virgo cluster the blue luminosity grows more slowly than the third power of distance (see §4.5) as the local over-abundance of galaxies blends into the homogeneous distribution at larger scales.

An important assumption in our correction for completion is that the spatial distribution of the missing luminosity follows the spatial distribution of the recorded galaxies. This approximation is best where the fraction of uncatalogued luminosity is lowest: i.e., where the missing luminosity is dominated by the recorded luminosity. At large distances the opposite is true and we expect this approximation to be less accurate. Nevertheless, the specific nature of the spatial distribution at these distances is negligible for initial LIGO, where only small fractions of detections for initial LIGO will be due to galaxies at these large distances.

2.3. The chirp mass and its distribution

The GW inspiral signal depends, to leading order, on the so-called chirp mass, denoted \mathcal{M} :

$$\mathcal{M} \equiv \mu^{3/5} M^{2/5}, \quad (3)$$

where μ is the system’s reduced mass and M its total mass. To complete our specification of the physical compact object binary population we must characterize the populations distribution with chirp mass.

We model the distribution of compact object binary systems with component masses using the StarTrack (BKB) binary synthesis code. We use the resulting chirp mass distribution to determine the signal strength from a given binary at our GW detector. For example, Figure 2 (which also appears in Bulik & Belczynski 2003) shows the distribution of BCO chirp masses as calculated using the StarTrack binary synthesis code and BKB reference model A. (While we confine attention to reference model A in this section, we explore the dependence of the observed rates and distributions on the full range of BKB reference models

in §4.5.)

3. The distribution of BCOs anticipated in observations

Here we use the model for the physical BCO population developed in the previous section to determine the observed coalescence rate and distribution as a function of the detector’s noise characteristics.

The strength of the BCO inspiral signal observed in a detector system is characterized by the signal-to-noise ratio ρ which depends on the detector’s noise spectrum and the BCO chirp mass, distance, sky position, and orbital inclination. Detected binary systems will have signal-to-noise greater than a threshold ρ_0 .

For ground-based GW detectors like LIGO the signal from a coalescing compact object binary system persists in the detector for on-order seconds. Over that period the accumulated signal-to-noise will depend on the detector’s noise spectrum and the binary system’s distance, orbital plane inclination with respect to the detector line-of-sight, location on the detector’s sky, and a function — the so-called “chirp mass” (cf. eq. 4b) — of the binary’s component masses. The population model described in the previous section thus determines all the parameters necessary to evaluate whether a given binary system will be observed by, e.g., the LIGO detector system.

First predictions for the chirp mass distribution of observed systems were recently obtained by Bulik & Belczynski (2003), which considers varying underlying binary parameters. Additionally, Bulik, Belczynski, & Rudak (2004) studied the influence of different cosmological models on the observed chirp mass distribution. Complementing these studies, we determine the distribution of observed systems from the same physical BCO population model, however we include the effects of anisotropic distribution of galaxies while we do not consider the different underlying cosmological assumptions. Our method is as follows.

We first draw a representative sample of binary systems populating each galaxy; we evaluate the expected signal-to-noise in the detector system; we determine the observed population by choosing the subset of systems whose signal-to-noise in the detector system is greater than the detection threshold. Throughout this work we assume a signal-to-noise threshold for detection ρ_0 equal to 8. The results presented in this work are based on $\simeq 10^6$ binaries drawn randomly from $\simeq 75000$ galaxies. The ratio of the observed number of systems to the number of systems in the parent population defines the detection efficiency. The rate of detected inspiral events is equal to the merger rate in the physical population reduced by the detection efficiency.

3.1. Signal-to-Noise Ratio

The strength of a signal event observed in a detector is characterized by the event’s signal-to-noise ratio ρ . The anticipated ρ value associated with a particular source depends on the detector, the source, and the method of data analysis. For coalescing compact object binaries there is an optimal method of analysis — matched filtering — that allows us to express the *anticipated* ρ for a particular binary system in terms of its distance, component masses, and orientation with respect to the detector. Even for identical sources the actual signal-to-noise ratio will vary from instance to instance owing to the stochastic character of detector noise.

The expected signal-to-noise ρ associated with a compact object binary observed in a single detector using the technique of matched filtering was first derived by Finn & Chernoff (1993); here we use the particular expression as given in Finn (1996):

$$\rho_D \equiv 8\Theta \left(\frac{r_0}{D} \right) \left(\frac{\mathcal{M}}{1.2M_\odot} \right)^{5/6} \zeta(f_{\max}) \quad (4a)$$

where

$$\mathcal{M} = \mu^{3/5} M_{tot}^{2/5}, \quad (4b)$$

$$r_0^2 \equiv \frac{5}{192\pi} \left(\frac{3}{20} \right)^{5/3} x_{7/3} M_\odot^2, \quad (4c)$$

$$x_{7/3} \equiv \int_0^\infty \frac{df (\pi M_\odot)^2}{(\pi f M_\odot)^{7/3} S_h(f)}, \quad (4d)$$

$$\zeta(f_{\max}) \equiv \frac{1}{x_{7/3}} \int_0^{2f_{\max}} \frac{df (\pi M_\odot)^2}{(\pi f M_\odot)^{7/3} S_h(f)}, \quad (4e)$$

D is the luminosity distance to the binary system, Θ is a function of the relative orientation of the binary (including its orbital plane inclination) and the detector, M and μ are the system’s total and reduced mass, $S_h(f)$ is the detector noise power spectral density in units of squared GW strain per Hz, and f_{\max} is the GW frequency at which the inspiral detection template ends (and which is no greater than the frequency at which the inspiral itself transitions into coalescence).

The LIGO detector system consists of not one but three detectors: a 4 Km interferometer (H1) and a 2 Km interferometer (H2) located near Hanford, Washington, and a 4 Km interferometer (L1) located near Livingston, Louisiana. The signal-to-noise associated with any given inspiraling BCO will be different in the three interferometers, owing to differences in their respective noise power spectral densities S_h and their geographic locations and orientations. When we speak of the signal-to-noise associated with an compact object binary

inspiral observed in LIGO we will assume that these three interferometers are used together as a single detector following Finn (2001b), in which case the signal-to-noise ratio for the network of three detectors can be approximated, for LIGO, by the quadrature sum of the signal-to-noise ratios in the individual detectors:

$$\rho^2 = \rho_{\text{H1}}^2 + \rho_{\text{H2}}^2 + \rho_{\text{L1}}^2, \quad (5)$$

where ρ_{H1} , ρ_{H2} and ρ_{L1} refer to the expected signal to noise of the binary in the H1, H2 and L1 detectors, calculated via 4a, respectively.

In the following subsections we discuss ζ , f_{max} and Θ in more detail.

3.2. ζ and f_{max}

The chirp mass \mathcal{M} and frequency f_{max} are intrinsic properties of the BCO. The GW signal from an inspiraling binary system is nearly sinusoidal with a frequency twice the binary’s orbital frequency. Consequently, over time the signal enters the detector’s effective bandwidth from low-frequency, travels across the band as time elapses, and — if the frequency where the inspiral ends and coalescence takes place is high enough — leaves the detector’s bandwidth at high frequency. The quantity $\zeta(f_{\text{max}})$ is unity when the BCOs inspiral phase completely covers the detectors effective bandwidth and is less than unity to the degree that the inspiral terminates within the detectors band, or before the signal enters the band.

We model f_{max} by assuming that the BCO inspiral phase proceeds until an *innermost circular orbit* (ICO) is reached, at which point the components coalesce in less than an orbital period. Using the post-Newtonian approximation together with a compelling ansatz Kidder, Will, & Wiseman (1993) have estimated the ICO orbital frequency for binaries with components of equal mass to be

$$f_{\text{ICO}} = 710 \text{Hz} \left(\frac{2.8 M_{\odot}}{M} \right). \quad (6)$$

We assume that f_{max} is equal to f_{ICO} .

For binaries with unequal mass components, f_{ICO} depends additionally on a function of μ/M . For the binaries that we encounter in our Monte Carlo procedure (where the mass ratio of the larger over the smaller is rarely above 2.5), the effect of the mass asymmetry is small. We ignore this small correction, making exclusive use of eq. (6).

The question of how the transition from inspiral to coalescence takes place is far from settled. The Kidder, Will, & Wiseman (1993) calculation of f_{ICO} treats the binary components as point masses, ignores hydrodynamic effects, and employs an ansatz that — while

compelling — is still a guess, based on an analogy to Schwarzschild spacetime. A number of authors have discussed hydrodynamic effects that may lead to coalescence at orbital frequencies less than f_{ICO} (Faber, Grandclement, Rasio, & Taniguchi 2002; Lai & Wiseman 1996; Lai, Rasio, & Shapiro 1994), and numerical simulations of relativistic binary systems have led to other results for the f_{ICO} orbital period (Taniguchi & Gourgoulhon 2002; Grandclement et al. 2002; Cook 2002; Baumgarte & Shapiro 2003). Future work will need to explore the dependence of the observed rates and chirp mass distribution on this uncertainty as well.

3.2.1. The Antenna Projection Θ

Interferometric detectors like LIGO are sensitive to a single GW polarization and have a quadrupole antenna pattern (Thorne 1987). The function Θ , defined in detail in Finn & Chernoff (1993); Finn (1996) describes the dependence of the inspiral signal-to-noise ratio on the position and orientation of the binary relative to the detector. It ranges from 0 to 4, with typical values near unity *when we consider an isotropic distribution of sources*. In the local neighborhood, however, the distribution of galaxies is not isotropic on the detector’s sky: e.g., there are significant concentrations of galaxies in the direction of the Virgo and the Fornax clusters, which are at a fixed declination relative to the LIGO detectors. Since the signal-to-noise ratio of a binary is directly proportional to Θ , binaries from galaxies at some declinations are more likely to be detected than binaries in others and this plays an important role in relating the observed event rate to the underlying, physical event rate.

For example, Figure 3 compares the distribution of Θ for binaries associated with Virgo cluster galaxies (solid line) as observed at the LIGO Hanford detector to the distribution of Θ for binaries isotropically distributed about the sky. Note that Virgo is relatively poorly positioned in declination relative to the LIGO Hanford detector, leading to a smaller number of sources with large Θ than we would expect for an isotropic distribution of binaries.

3.3. The noise power spectral density $S_h(f)$

The influence of the detector on the signal-to-noise ratio ρ enters through the quantity r_0 and the function $\zeta(f)$, each of which depend on the detector’s strain-equivalent noise power spectral density $S_h(f)$ (cf. eq. 4).

A GW signal incident on an interferometric detector like LIGO leads to a response that can be characterized as a projection $h(t)$ of the incident GW strain acting on the detector

arms. Measurement noise, which is contributed at many points in the transduction chain, is indistinguishable from a GW signal $h_n(t)$ and we characterize the *strain-equivalent noise* by its mean square amplitude, $\overline{h_n^2}$. The strain-equivalent noise power spectral density $S_h(f)$ is the contribution to $\overline{h_n^2}$ from noise components in a 1 Hz bandwidth about the frequency f , so that

$$\overline{h_n^2} = \int_0^\infty df S_h(f). \quad (7)$$

LIGO is currently in the late stages of commissioning, with results from early data sets under review (Abbott et al. 2003a,b,c). When commissioning is complete the noise power spectral density $S_h(f)$ will meet or exceed the specification given in (Lazzarini & Weiss 1996, 3-2). To evaluate the sensitivity of the initial LIGO instrumentation we use a parameterized version of this noise curve (Owen 2001),

$$S_h(f) = 9 \times 10^{-46} [(4.49x)^{-56} + 0.16x^{-4.52} + 0.52 + 0.32x^2] \text{ Hz}^{-1} \quad (8)$$

$$x \equiv \frac{f}{150\text{Hz}}, \quad (9)$$

for each of the two LIGO 4 Km interferometers (referred to as H1 and L1). For the 2 Km Hanford detector (referred to as H2) we approximate $S_{h,2km}(f)$ as $4 S_{h(f)}$.⁴ As a consequence of this approximation note that for the initial LIGO detectors

- $\zeta(f_{\text{max}})$ is the same function of \mathcal{M} for H1, H2 and L1 approximation; and
- r_0 for H1 and L1 are identical and twice the appropriate for H2:

$$r_{\text{H1}} = r_{\text{L1}} = 2r_{\text{H2}} = 7.7 \quad (10)$$

The LIGO Laboratory and the LIGO Scientific Collaboration have also recently proposed an advanced set of LIGO detectors. In addition to extending the 2 Km Hanford interferometer to a full 4 Km these advanced detectors have a much lower detector noise and a greater effective bandwidth for BCO inspiral searches. We have also evaluated the event rates and distributions using the current estimates for the limiting noise sources associated with this advanced detector system (Shoemaker 2003, private communication). Figure 4 shows the target noise curve for the initial LIGO detectors (eq.[8]) and the current estimate for the advanced LIGO limiting noise curve. Again note that, as a consequence of this approximation

⁴Not all noise sources scale with length in a simple manner: in particular, the laser shot noise spectrum depends on the Fabrey-Perot arm cavities in a more complicated manner. Nevertheless this approximation is more than suitable for our purpose here.

- $\zeta(f_{\max})$ is the same function of \mathcal{M} for H1, H2 and L1 approximation; and
- r_0 for H1, H2 and L1 are identical for the advanced LIGO detectors:

$$r_{\text{H1}} = r_{\text{L1}} = r_{\text{H2}} \simeq 120 \quad (11)$$

4. RESULTS

In this section we discuss how the differential sensitivity of the LIGO detectors, as a function of source sky position, chirp mass, distance and analysis threshold, can be combined with the spatial and chirp mass distribution of coalescing binaries, to determine how the observed coalescing binary distribution reflects the underlying, physical distribution.

4.1. Binary Compact Object Populations in Galaxies

In addition to its dependence on distance, sky position and orbital plane inclination, the sensitivity of GW detectors like LIGO to a particular BCO depends on a function of the binary’s component masses. We use the BKB binary synthesis calculations to populate each galaxy with a distribution of binary systems of different chirp mass⁵. The luminosity scaling of Phinney (1991) is naturally applicable to our approach and we set the total inspiral rate for a particular galaxy equal to the Milky Way rate $R_{\text{det,MW}}$ times its blue luminosity (corrected for reddening) in units of the Milky Way blue luminosity. Note that $R_{\text{det,MW}} = R_{\text{MW}}$, since the initial LIGO detectors are expected to detect essentially all BCO inspirals in the Milky Way with chirp mass less than $18 M_{\odot}$ (that exceeds the typical expected maximum chirp mass; see Figure 2).

$$\mathcal{R}_{\text{gal}} = \frac{L_{\text{gal,b}}}{L_{\text{MW}}} R_{\text{MW}}. \quad (12)$$

Our principal tool for understanding how the physical distribution of coalescing binaries is reflected in the observed distribution is the detection efficiency. We define the detection efficiency as the fraction of binaries from a given population that are detected with a signal-to-noise ratio higher than a chosen threshold (in this study: 8). We may thus consider the

⁵For the most part of §4, we confine our attention to the reference model A from BKB. However we explore the full set of BKB models in §4.5

detection efficiency for all binaries in a given galaxy, or the efficiency for NS-NS binaries over all galaxies, or the efficiency for detection of binaries at a given sidereal time, etc.

Under the assumption of uniform galaxy distribution, the natural measure of a detector’s sensitivity is the volume of space surveyed, which is conveniently expressed as an effective radius r such that the surveyed volume is equal to the volume of a sphere of radius r (Finn 2001a). When taking into account the actual galaxy distribution and the variation in binary populations among galaxies a different measure of sensitivity suggests itself: the effective number of Milky Way galaxies surveyed,

$$N_G \equiv \frac{R_{\text{det}}}{R_{\text{MW}}} = \sum_i \frac{L_i}{L_{\text{MW}}} f_{\text{det},i}, \quad (13)$$

where $f_{\text{det},i}$ is the detection efficiency and L_i is the blue luminosity for galaxy i , L_{MW} is the Milky Way’s blue luminosity, and we have used the blue luminosity scaling L_i/L_{MW} as discussed in §2.2. The concept of N_G is more appropriate for our approach, since it takes into account the actual galaxy distribution and the BCO mass distribution. As detectors become more sensitive, N_G grows accordingly.

In this formulation $R_{\text{det}} = N_G R_{\text{MW}}$. The Galactic inspiral rate R_{MW} can be calculated based on the current observed sample for NS-NS (Kalogera et al. 2003) and from population synthesis calculations (e.g., BKB).

4.2. Detection efficiency and sidereal time

Interferometric detectors like LIGO are most sensitive to gravitational waves of a single polarization incident normal to the plane of the detector’s arms. As the Earth rotates about its axis, the sky locations and polarization of sources to which it is most sensitive rotate as well. Since galaxies are not uniformly distributed about the sky the expected rate of detected coalescence events is periodic with the sidereal day. The detailed variation depends on the geographical distribution of galaxies, the distribution of coalescing binaries with system chirp mass, and the signal-to-noise threshold for detection. Figure 5 shows the probability density for detections under the assumptions that the geographical distribution of galaxies is determined by our galaxy catalog approach (cf. §2.2.1), the chirp mass distribution of coalescing binaries is given by BKB model A, and the signal-to-noise ratio ρ_0 threshold for detection in initial LIGO is 8. Here time t is measured in hours and is given by UT plus the sidereal time at Greenwich at 0h UT. The Virgo Cluster is above a point in between the Hanford and Livingston detectors for approximately the duration $18h < t < 20h$, closely coinciding with the peak in Figure 5.

4.3. Dependence of detection range and efficiency on declination

Setting aside the actual distribution of galaxies, it is interesting to note the dependence of the detectors “range” — or distance to the most distant observable source above threshold — on source sky position. When sampled over sidereal time, the range depends on the sky position only through declination. Figure 6 shows, for initial LIGO, the detector range as a function of declination, normalized to $1.4 + 1.4 M_{\odot}$ NS-NS binaries. For an advanced LIGO with the H2 interferometer extended to 4 Km the declinations of maximum range will shift slightly toward the zenith and nadir of L1.

Figure 7 shows the dependence of detection efficiency — i.e., the fraction of binaries detected — on declination for galaxies at the distance of the Virgo cluster. Note that this dependence on declination will change if the ground-based detectors are located differently. In particular, the sensitivity of detectors to inspirals from the Virgo cluster improves for detectors with latitudes corresponding to declinations near that of Virgo. Indeed, Livingston and VIRGO, due to the relative proximity of their latitude and the Virgo cluster’s declination, are more optimally placed relative to the Virgo cluster than the Hanford or GEO detectors. Interestingly, had H1 and H2 been constructed exactly as they are, but instead with the present latitude of the VIRGO detector, the LIGO network would detect about 25% more NS-NS inspirals (at design sensitivity) from the Virgo cluster.

Note that the maximum detection efficiency at this distance in Figure 7 occurs for galaxies located at the celestial poles. This might be surprising since the detectors are most sensitive to sources at their zenith or nadir. The reason for this apparently paradoxical result is that a galaxy at a declination corresponding to the detector latitude is only at the detector’s zenith for a short fraction of a sidereal day, while the efficiency for galaxies at a celestial pole are independent of sidereal time. Despite the shorter duty cycle for sources at the detector zenith or nadir, it is still the case that galaxies at these locations will be seen to greater distances.

4.4. Dependence of detection efficiency on both galaxy and BCO mass distributions

Figure 8 shows the detection efficiency of every galaxy in our catalog, plotted as a function of galaxy distance. The top panel shows the total efficiency for the complete population of binaries. Subsequent panels shows the efficiencies for the BH-BH, NS-BH and NS-NS sub-populations for initial LIGO. Galaxies at a given distance have a range of efficiencies owing to their different declinations. This may amount to as much as a 40% variation.

Previous studies adopted a detection efficiency for initial LIGO of unity up to distances of 20 Mpc for NS-NS, 40 Mpc for NS-BH, 100 Mpc for BH-BH, and 46 Mpc for the entire population, and zero beyond. These cut-offs are shown as vertical dashed lines. In our more realistic approach one sees non-zero efficiencies to much greater distances. For example BH-BH binaries are observed with 10% efficiency even at distances of 130 Mpc. On the other hand, inside the previously adopted cut-off distances the efficiency is not 100%: for example, the overall efficiency to Virgo cluster inspirals is 60%.

The NS-NS, NS-BH and BH-BH sub-population efficiencies vary differently with distance owing to their different chirp mass distributions. Figure 9 shows the expected distribution with chirp mass of detected binaries. This should be contrasted with the actual population distribution, as shown in Figure 2. As expected the distribution is dominated by BH-BH binaries; however, the relative proportion of detected NS-NS binaries is more than double the proportion previously calculated assuming a uniform galaxy distribution (Bulik & Belczynski 2003). The increased proportion of NS-NS relative to BH-BH binaries arises because the uniform galaxy distribution assumption significantly underestimates the number of galaxies in the nearby universe. As is apparent from Figure 1, this underestimate is greater at Virgo cluster distances, where there is still significant efficiency for NS-NS binaries, than at, e.g., 100 Mpc where only BH-BH are detected. Correspondingly, the boost in the number of NS-NS binaries, relative to the uniform distribution model, is greater for NS-NS binaries than it is for BH-NS binaries and for BH-BH binaries. (The sensitivity of the advanced LIGO detectors is sufficiently great that the uniform assumption is applicable and the distribution of detected sources will follow Bulik & Belczynski (2003) more closely.) From Figure 9 we also note that about half of the detected binaries are expected to have chirp mass in the range $5 - 9 M_{\odot}$, with a peak at $9 M_{\odot}$ (corresponding to $2 \times 10 M_{\odot}$ black holes). These results can be folded with the most current Galactic rate estimates to estimate the number of black hole inspiral events with chirp masses in the above range that we might expect from initial LIGO observations in one year at full sensitivity. It is clear that data searches would need to focus on these higher masses, where however the GW waveforms are harder to calculate. Nevertheless the necessary effort with focus on these systems is needed, since limits in this range will be most constraining to population models.

4.5. Effective number of MWEG surveyed

The naive use of an effective radius can lead to a misunderstanding in the overall rate and nature of detected coalescing binary systems. Figure 10 shows the cumulative rate of detections by the initial LIGO detector from sources within a distance D . The dashed line

shows the cumulative rate assuming a uniform distribution of galaxies and a 100% efficiency for binaries within a distance r , with r equal to 20, 40, and 100 Mpc, for NS-NS, NS-BH, and BH-BH binaries respectively. The solid line show the approach taken here: i.e., the rate of detected binaries within a distance D taking into account the actual galaxy distribution, the estimated number of binaries per galaxy, the distribution of binaries with chirp mass, and the overall detection efficiency for each galaxy. The solid lines show evidence that particular geographic features in the distribution of galaxies have sharp effects on rate of detections. The most striking example is the Virgo Cluster (the spike at 20 Mpc), which comprises, for example, 20% of NS-NS detections. In general, NS-NS extrapolation factors based on the uniform galaxy density assumption have been underestimated by a factor of $\simeq 2 - 3$, while BH-BH extrapolation factors have been slightly overestimated by a factor $< 100\%$.

Even though the quantity N_G is *normalized* to the Galactic rate, it still depends on the assumed model chirp mass distribution. To examine this dependence we consider all models calculated in BKB that are considered realistic at present. We calculate the associated N_G values for each of the three BCO populations shown in Figure 11. These models differ in terms of a number of parameters that determine single-star and binary evolution (e.g., stellar winds, common envelope evolution, NS and BH kicks, etc; for a detailed discussion see BKB). Based on these models it is evident that the variation in N_G is lower than a factor of 1.5-2 for the three types of BCO populations. We consider these variations to represent the systematic uncertainty associated with the extrapolation factor N_G .

Finally, we explore the growth of N_G with detector sensitivity. As LIGO’s sensitivity improves, approaching design sensitivity for initial and advanced detectors, of particular interest is the growth of N_G for NS-NS binaries. In lieu of a detection, N_G is important for assessing upper rate limits for NS-NS inspiral in the Milky Way. A measure of the sensitivity improvement is the increase of the value of r_0 (see eq. 4c) or the ratio

$$\xi \equiv \frac{r_0}{r_{0,SRD}}, \tag{14}$$

where $r_{0,SRD}$ is calculated similarly but with the advanced LIGO noise curve. In Figure 12 we show the dependence of N_G on ξ for the initial LIGO configuration of 4 and 2 km detectors in Hanford, Washington, and a 4 km detector in Livingston, Louisiana. The effective number of MWEG surveyed increases as x^P , initially with $P < 1$, but growing with $P \simeq 2.6$ as design sensitivity is reached. This rate represents an increase by a factor of $\simeq 300$ Milky Way equivalent galaxies compared to the sensitivity of the detectors during the first Science Run (Abbott et al. 2003a).

5. CONCLUSIONS

In anticipation of the development of GW astrophysics in the next several years, we consider the effects of observational selection effects on the detectability of BCO inspiral events. Our primary goal is to develop a realistic framework for the astrophysical interpretation of rate constraints (from upper limits or inspiral detections) anticipated in the next few years. This interpretation should account for the main selection effects associated with ground-based GW observations and properly constrain models of radio pulsar and BCO populations. As a result of our calculations we also make realistic estimates for the extrapolation of Galactic inspiral detection rates based on the known spatial distribution of galaxies in the nearby universe and the expected mass distributions of binary compact objects.

Our results are summarized as follows:

- The local distribution of galaxies mostly relevant to NS-NS detections with initial LIGO is in fact very different from isotropic in sky direction and volume density. Most importantly the Virgo cluster represents a significant step in the cumulative blue luminosity (or the cumulative number of MWEG) all concentrated at a given (rather unfortunate) sky position. Failure to properly account for this local distribution of BCO sources would lead us to underestimating the importance of an upper limit on the inspiral rate derived from GW observations.
- Until this study, because of the assumption of isotropic distribution of galaxies, detection rates of NS-NS inspirals have been underestimated by factors of 2 – 4 and BH-BH inspirals have been *overestimated* by nearly a factor of 2. These factors include the systematic uncertainties due to the chirp-mass distributions that are not very well constrained.
- Detections of inspiral events and measurements of compact object masses are expected to provide us with tighter constraints on the BCO mass distributions and thus on the physics of BCO formation. However, our analysis shows that mass distributions of detected BCOs are strongly skewed towards higher masses (because of their stronger signals) compared to the parent mass distribution (see Figures 2 and 9). For our reference population model, we find that about half of detected inspirals correspond to binaries with high chirp masses ($5 - 9 M_{\odot}$). Since event rate limits in this range will be most constraining to BCO models, it is evident that there is a need for the development of efficient search methods for such massive systems. Understanding the systematics of this bias will be crucial for the astrophysical interpretation of such detections.
- Inspiral detection efficiency depends strongly on the host galaxy sky position and the

binary orbit orientation with respect to the detectors; as a result the true maximum distance for an optimally oriented binary can exceed the average detection distance by more than a factor of two.

- Using the current most favorable (at peak probability) estimates of NS-NS inspiral rates for the Galaxy (Kalogera et al. 2003) and our results on N_G values, we find expected initial LIGO detection rates in the range of one event per 200 – 3 years (for the reference pulsar population model at 95% confidence level the range is one event per 3 - 50 years).

From the various galaxy physical properties we have considered the blue luminosity (corrected for reddening), but we have ignored galaxy metallicity and star formation history. Both of these factors affect the expected mass distribution of compact object binaries as well as their birth rate, for a given luminosity. For example, metallicity affects massive stellar winds and the final compact object masses. This effect has already been taken into account in Abbott et al. (2003c) where the Magellanic clouds have been reached by LIGO. In principle we would like to include these effects in our calculations (to the extent of our current understanding of binary evolution and how it is affected by these factors); however at present it does not seem possible since this information is not available in detail for every galaxy in the catalogs, and we chose to ignore these factors instead of include them for only a very small subset of sample.

With the work presented here we also advance a paradigm for using initial LIGO binary inspiral to constrain models of binary evolution and BCO formation and of pulsar population properties. Using the current estimates of NS-NS inspiral rates in MWEG (Kalogera et al. 2003) and scaling to the BH-BH population, it is clear that LIGO should eventually provide an astrophysically significant bound on the rate of BH-BH inspirals in the nearby universe. In the context of a particular binary synthesis model, such a bound can be translated to a bound on the MWEG BH-BH inspiral rate as well as on the rate for the NS-NS and NS-BH sub-populations. The derived bound on the NS-NS sub-population can be compared to the estimates that arise from binary pulsar observations (Kalogera et al. 2003). Note that GW observations may also directly bound the coalescence rate for the NS-BH and NS-NS sub-populations at a significant level. All these bounds will be consistent only for certain binary formation and synthesis models. In this way, GW observations will contribute to our understanding of compact binary formation and evolution.

This work is partially supported by National Science Foundation awards PHY 01-21420 (VK), PHY 00-9959 (LSF), and PHY 01-14375 (LSF, PN and VK), and a David and Lucile Packard Science & Engineering Fellowship (VK). KB acknowledges support of the grant

PBZ-KBN-054/P03/2001. PN and VK are also grateful for the warm hospitality of the Center for Gravitational Wave Physics at Penn State. The Center for Gravitational Wave Physics is funded by the NSF under cooperative agreement PHY 01-14375.

REFERENCES

- Abbott, B., et al. 2003. gr-qc/0308043.
- Abbott, B., et al. 2003. gr-gc/0308050.
- Abbott, B., et al. 2003. gr-gc/0308069
- Amaldi, E., et al. 1986, Nuovo Cimento, 9C, 829
- Ando, M., et al. 2001, Phys. Rev. Lett., 86, 3950
- Arzoumanian, Z., Cordes, J.H., Wasserman, I. 1998, ApJ, 520, 696.
- Astone, P., et al. 1993, Phys. Rev. D, 47, 362
- Astone, P., et al. 1997, Astroparticle Physics, 7, 231
- Baumgarte & Shapiro 2003, Physics Reports, 376, 41
- Belczynski, K., Kalogera, V., Bulik, T. 2002, ApJ, 572, 407 (BKB)
- Bonazzola, S., Gourgoulhon, E. 1996 A&A, 312, 675
- Bulik, T., Belczynski, K. 2003, ApJ, 589, L37
- Bulik, Belczynski, & Rudak 2004, A&A 415, 407
- Burgay et al. 2003, Nature (submitted)
- Caron, B. et al. 1997, Nucl. Phys., B54, 167
- Cook G.B. 2002, Phys. Rev. D65, 084003
- Curran, S.J., & Lorimer, D.R. 1995, MNRAS, 276, 347
- de Vaucouleurs, G., de Vaucouleurs, A., Corwin, H.G., Buta, R.J., Paturel, G., Fouque, P. 1991, Third Reference Catalog of Bright Galaxies. Springer-Verlag, New York
- Di Nella, H., Montuori, M., Paturel, G., Pietronero, L., Sylos Labini, F. 1996, *Å*, 308L.33D
- J. A. Faber, P. Grandclement, F. A. Rasio, & K. Taniguchi, Phys. Lev. Lett. 89, 231102
- Finn, L.S. & Chernoff, D.F. 1993, Phys. Rev. D, 47, 2198
- Finn, L.S. 1996. Phys. Rev. D, 53(6), 2878

- Finn, L.S. 2001, in Proc. AIP conf., 575, 92, Melvill, New York
- Finn, L.S. 2001, Phys. Rev. D, 63, 102001
- Grandclement P., Gourgoulhon E., Bonazzola S., 2002, Phys. Rev. D65, 044021
- Hulse, R.A., & Taylor, J.H. 1974, ApJ, 191, L59
- Kalogera, V., Narayan, R., Spergel, D.N., Taylor, J.H. 2001, ApJ, 556, 340
- Kalogera et al. 2003, ApJL, in press
- Kidder, L.E., Will, C.M., Wiseman, A.G. 1993, Phys. Rev. D, 47(8) ,3281
- Kim, C., Kalogera, V., Lorimer, D. R. 2003, ApJ, 584, 985
- Lai D., Rasio F. A., Shapiro S. L., 1994 ApJ, 420, 811
- Lai D., Wiseman A. G., 1996, Phys. Rev. D, 54, 3958
- Lazzarini, A., Weiss, R. 1996, LIGO Science Requirements Document (SRD), Internal LIGO Document
- Lazzarini, A., Mahjid, W. 1998, Galactic Distribution in Nearby Sky, Internal LIGO Document
- Lipunov, V. M.; Nazin, S. N.; Panchenko, I. E.; Postnov, K. A.; Prokhorov, M. E. 1995 \hat{a} 298, 677
- Mauceli, E., et al. 1996, Phys. Rev. D, 54, 1264–1275
- Narayan, R., Piran, T., Shemi, A. 1991, ApJ,379, L17
- Owen, B.J. 2001, private communication
- G. Paturel, P. Fouque, L. Bottinelli, L. Gouguenheim, \hat{a} 80, 299P
- Phinney, E.S. 1991, ApJ,380, L17
- Prodi, G. A., et al. 1998, Proceedings of the Second Edoardo Amaldi Conference on Gravitational Waves, ed. E. Coccia, G. Pizzella, and G. Veneziano (Singapore: World Scientific Press), Vol 4, pp. 148–158.
- K. Taniguchi and E. Gourgoulhon 2002, Phys. Rev. D 66, 104019
- Taylor, J.H. & Weisberg, J.M. 1989, ApJ, 345, 434

Thorne, K.S. 1987, in 300 Years of Gravitation, ed. Hawking, S. & Israel, W. (Cambridge: Cambridge University Press), 330-458

Tully, R.B., 1988, Nearby Galaxy Catalog. Cambridge Univ. Press

Tully, R.B., Astron. J. 96, 73

York, D. G. et al. 2000, AJ, 120, 1579

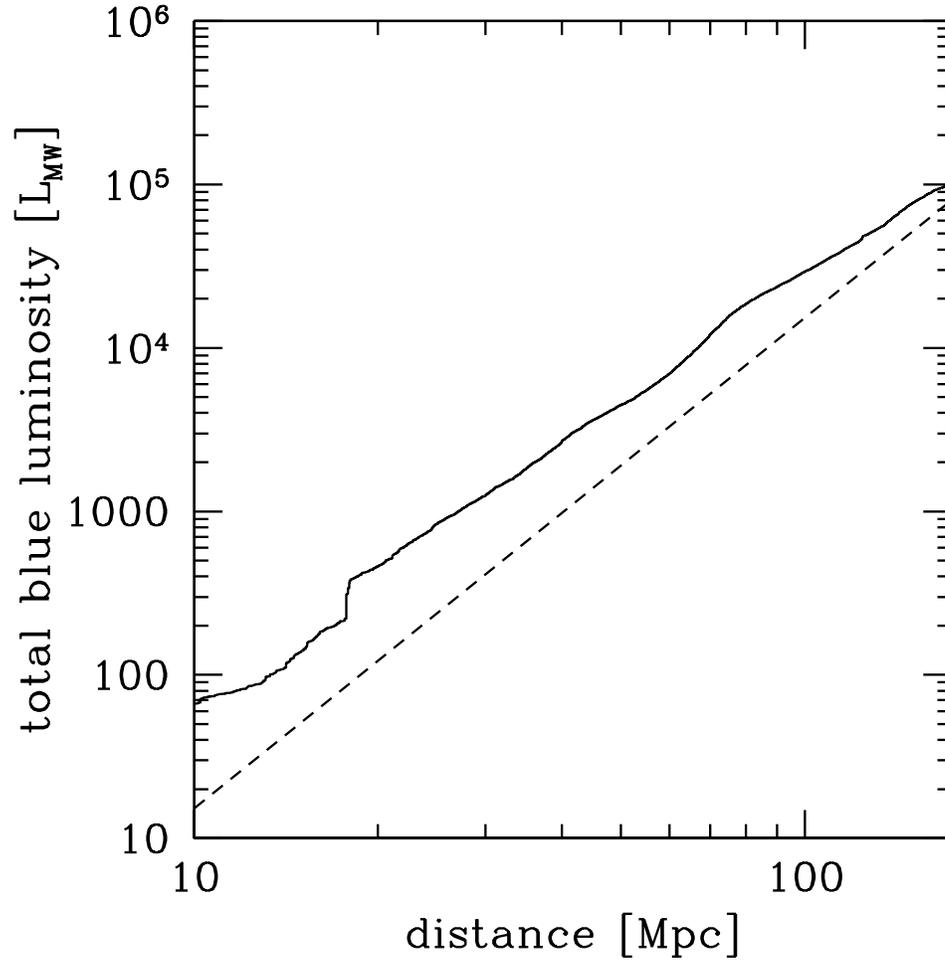


Fig. 1.— Cumulative blue luminosity enclosed within a distance D using the LEDA galaxy catalog and correcting for incompleteness. The dashed line is produced assuming a uniform distribution of luminosity in space (using the normalization density adopted in KNST).

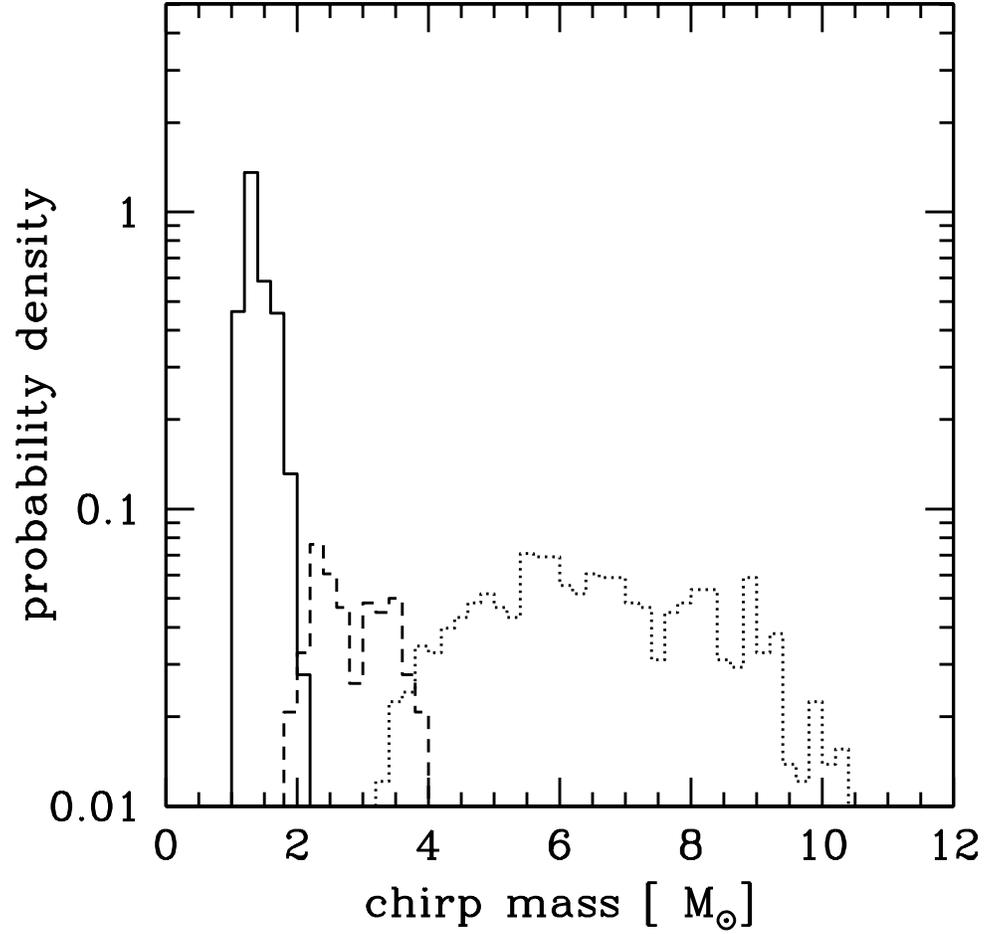


Fig. 2.— The chirp mass distribution for inspiraling binaries, using model A from BKB, NS-NS (solid), NS-BH (dashed), and BH-BH (dotted) binaries.

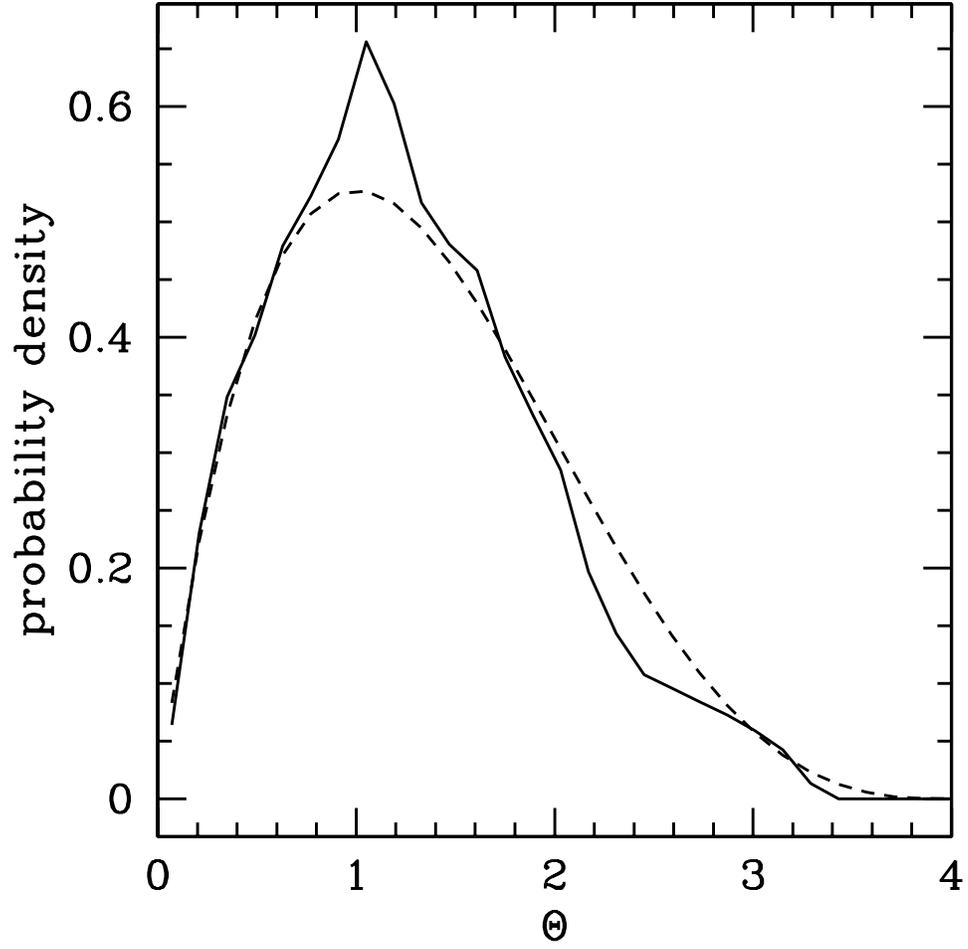


Fig. 3.— The normalized probability distribution of Θ . The solid line gives the distribution for inspirals from galaxies in the Virgo Cluster relative to LIGO Hanford. The dashed line gives the distribution assuming sources are uniformly distributed in space.

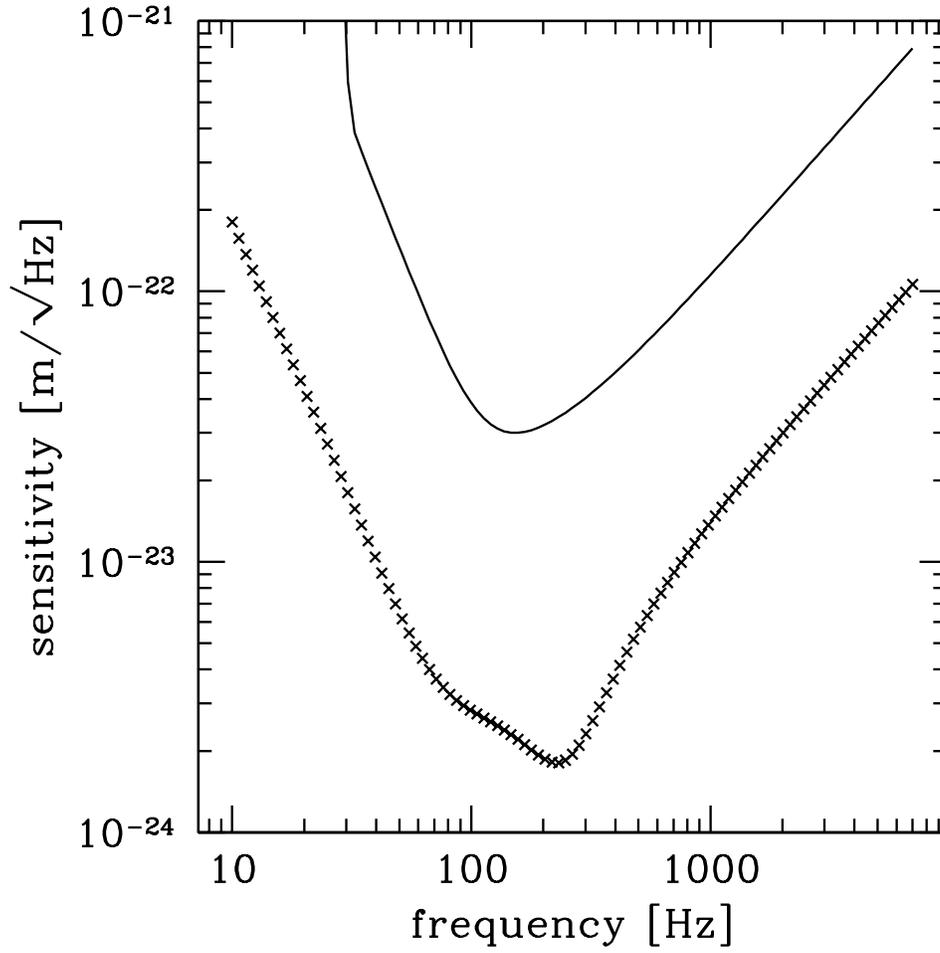


Fig. 4.— Target noise curves for Initial (solid line) and Advanced (crosses) LIGO detectors.

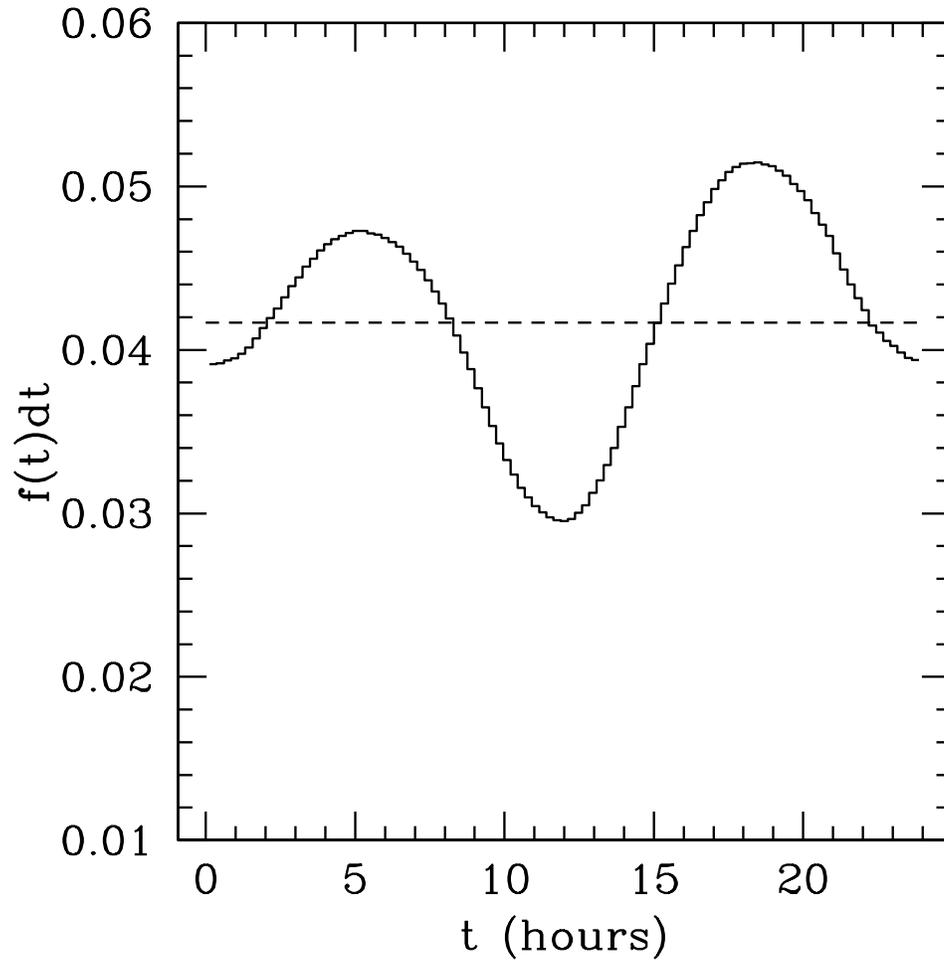


Fig. 5.— Probability $f(t)dt$ that an initial LIGO detection would come at an hour t during the day. t is the UT plus the sidereal time at Greenwich at 0 h UT. The probability assuming uniform spatial distribution of galaxies is given for comparison (dashed line).

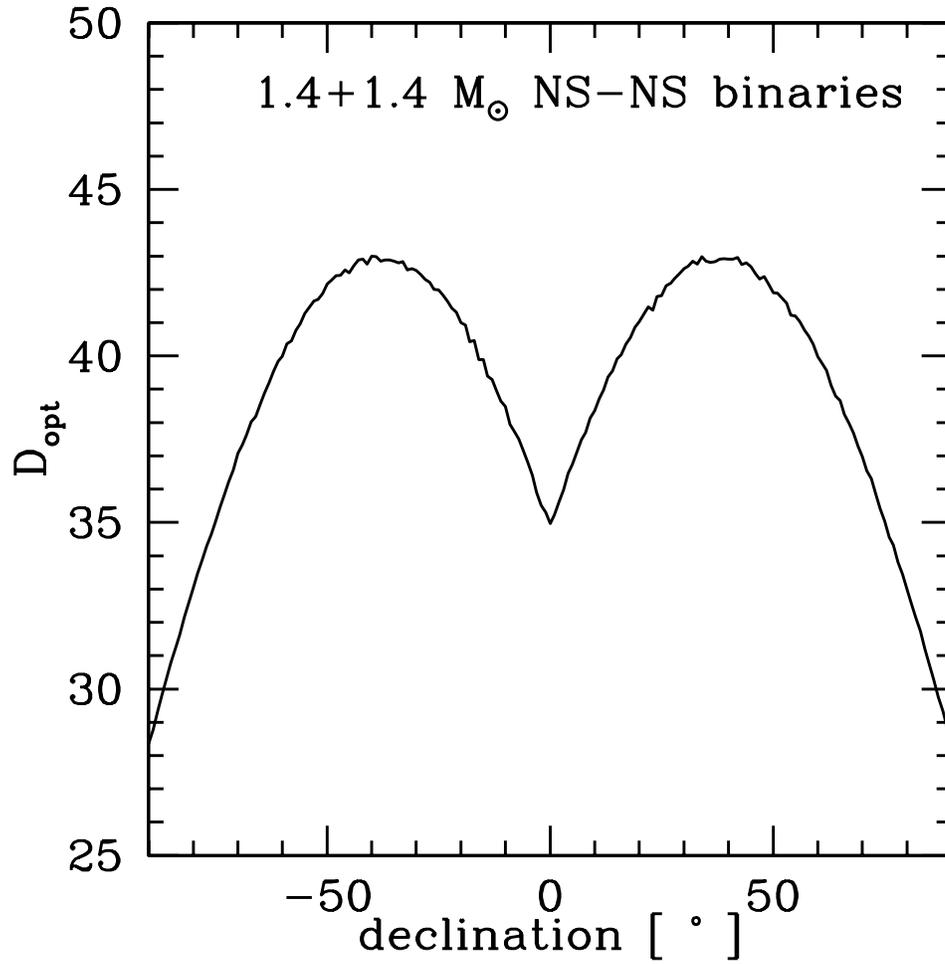


Fig. 6.— Maximum detection distance for the most optimally positioned binary as a function of declination. LIGO Hanford and LIGO Livingston have latitudes of $\simeq 45^\circ$ and $\simeq 30^\circ$ respectively. The peak in this plot corresponds to sources overhead a latitude in between the detectors, weighted more towards Hanford due to its two interferometers versus Livingston’s one.

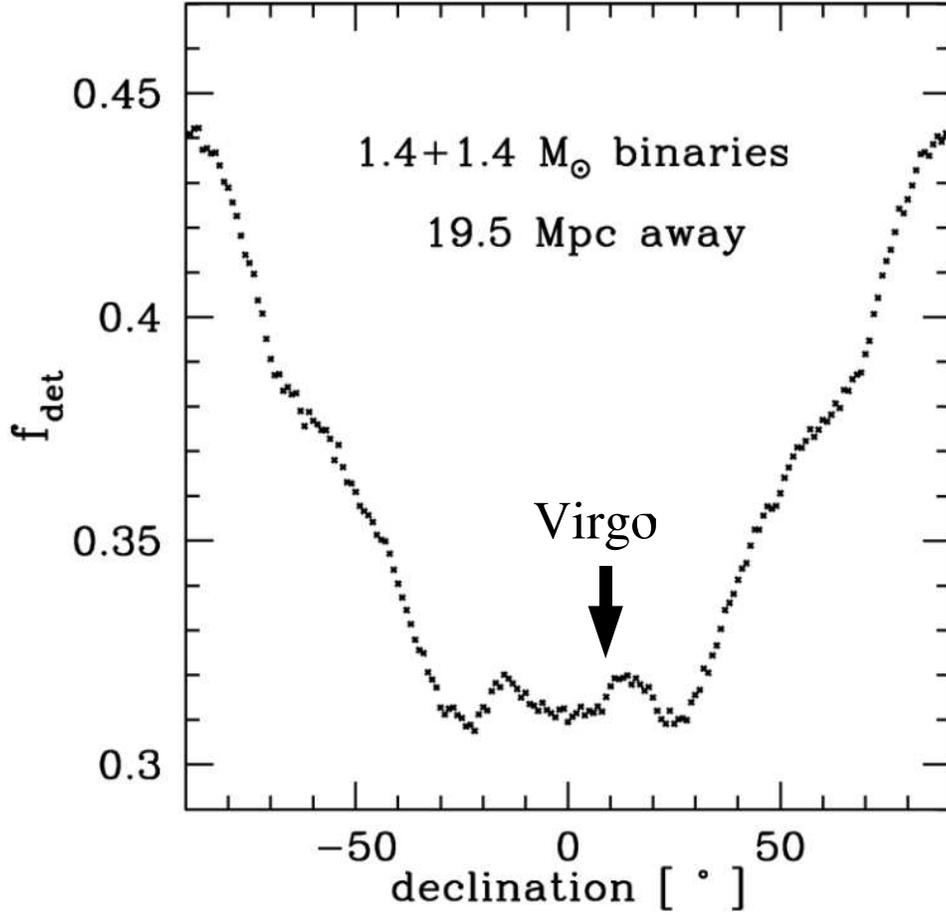


Fig. 7.— Detection efficiency as a function of declination, for $1.4 + 1.4 M_{\odot}$ NS-NS binaries. f_{det} is attenuated in regions near the equatorial plane, including the Virgo Cluster, which is a major source of NS-NS detections.

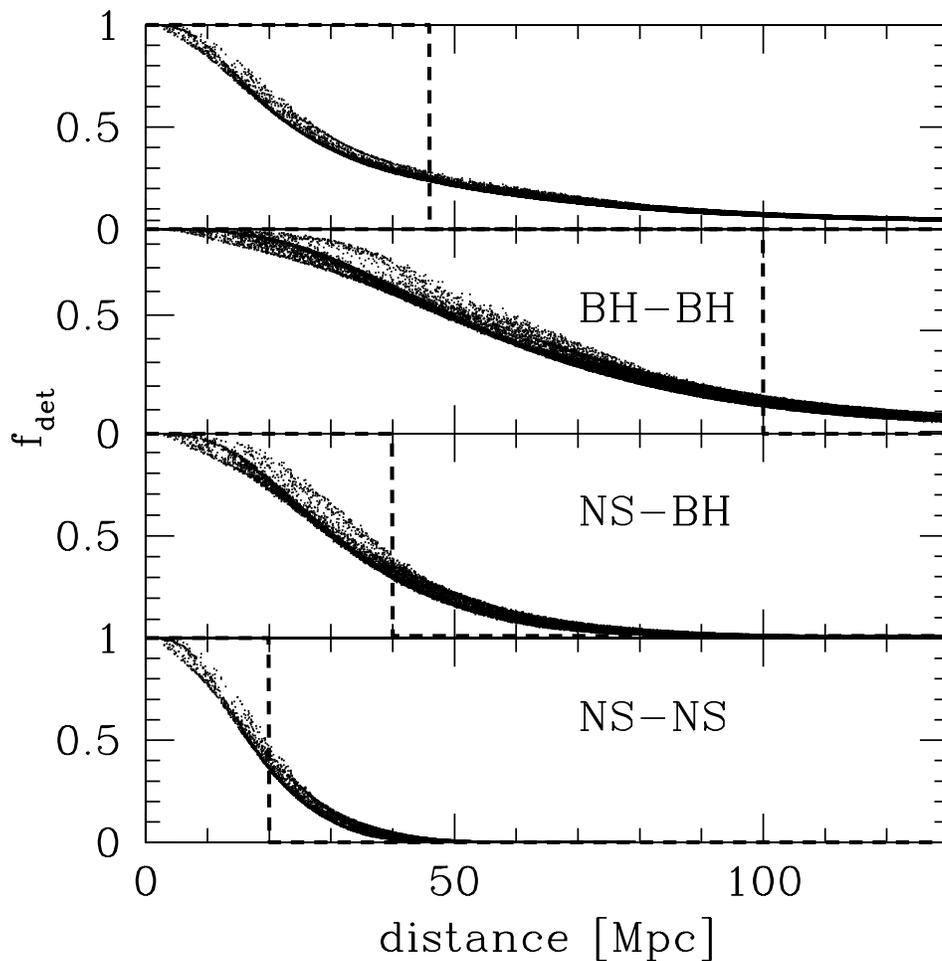


Fig. 8.— The detection efficiency of every galaxy in our catalog, plotted as a function of galaxy distance. The top panel shows the total efficiency for the complete population of binaries. Subsequent panels shows the efficiencies for the BH-BH, NS-BH and NS-NS sub-populations for initial LIGO. Previous studies adopted a step-like detection efficiency for initial LIGO at 20 Mpc for NS-NS, 40 Mpc for NS-BH, 100 Mpc for BH-BH, and 46 Mpc for the entire population: these cut-offs are shown as vertical dashed lines.

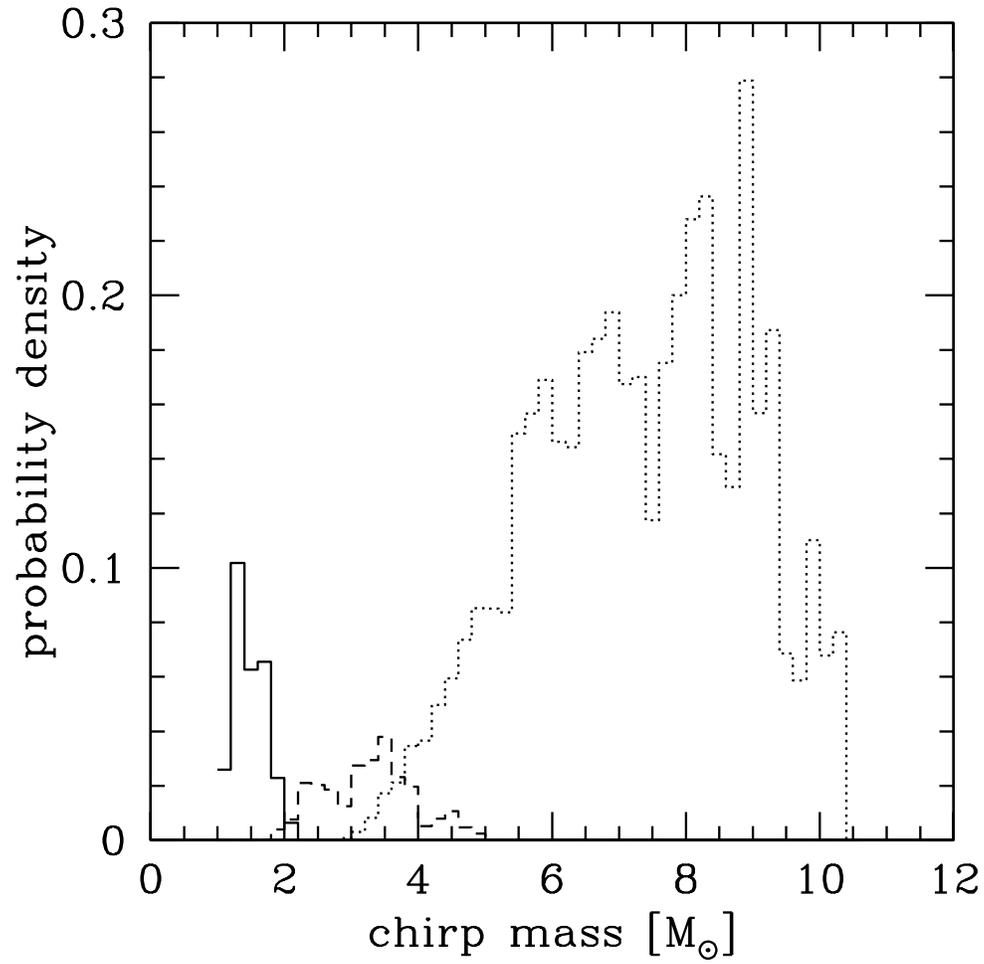


Fig. 9.— The expected normalized chirp mass distribution for detected inspirals, using model A from BKB. The solid line gives the NS-NS binaries, the dashed gives NS-BH binaries, the dotted gives BH-BH binaries. Compare to the intrinsic chirp mass distribution in Figure 2.

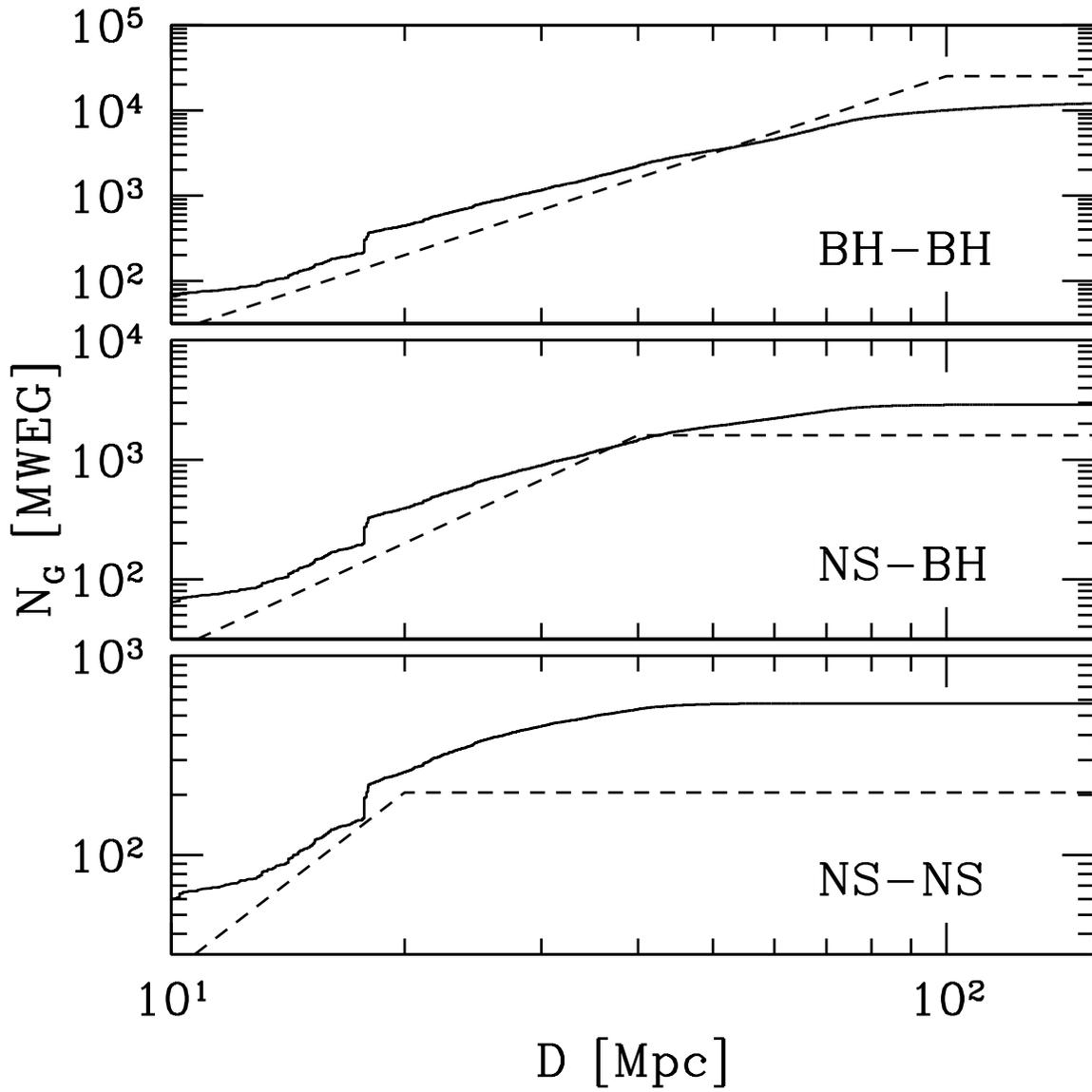


Fig. 10.— The effective number of Milky Way Equivalent Galaxies (MWEG) surveyed by initial LIGO, for events within a distance D for BH-BH (top), NS-BH (middle), and NS-NS (bottom) binaries. The dashed curves are calculated using the *uniform* approach adopting

maximum detection distances for NS-NS, NS-BH, and BH-BH at 20, 40, and 100 Mpc respectively. The solid curves are calculated using the *galaxy catalog* approach.

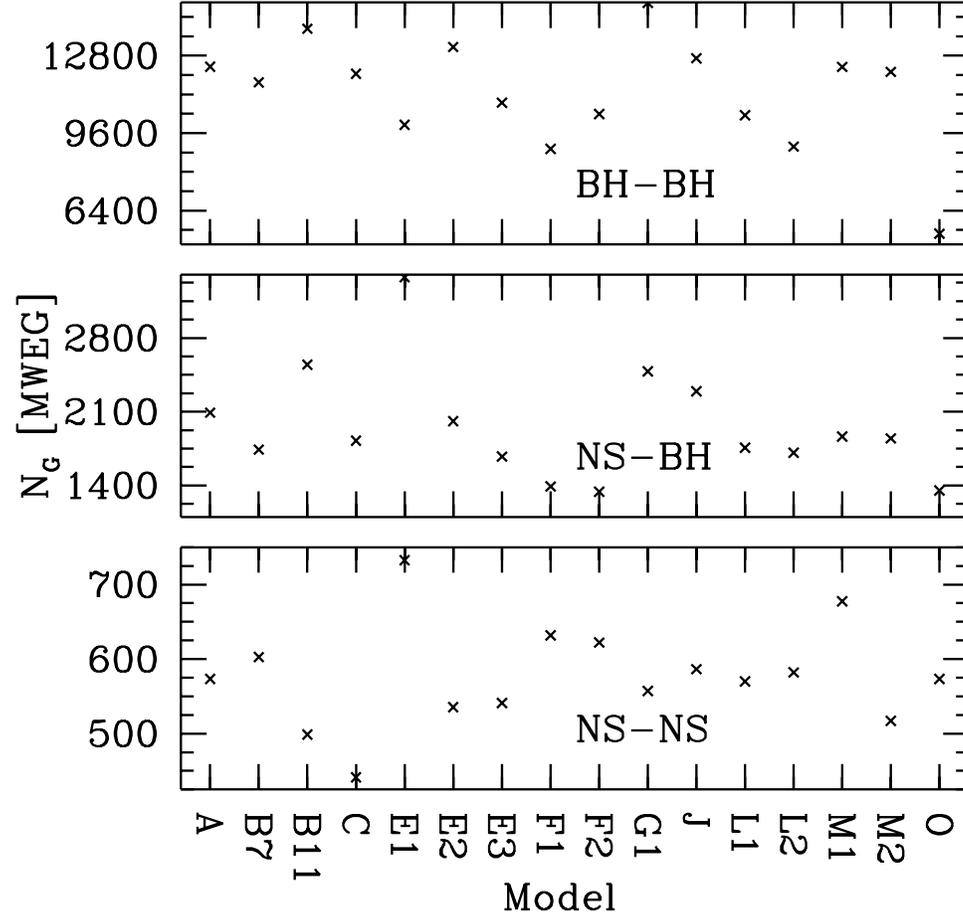


Fig. 11.— N_G for Different Population Synthesis Models.

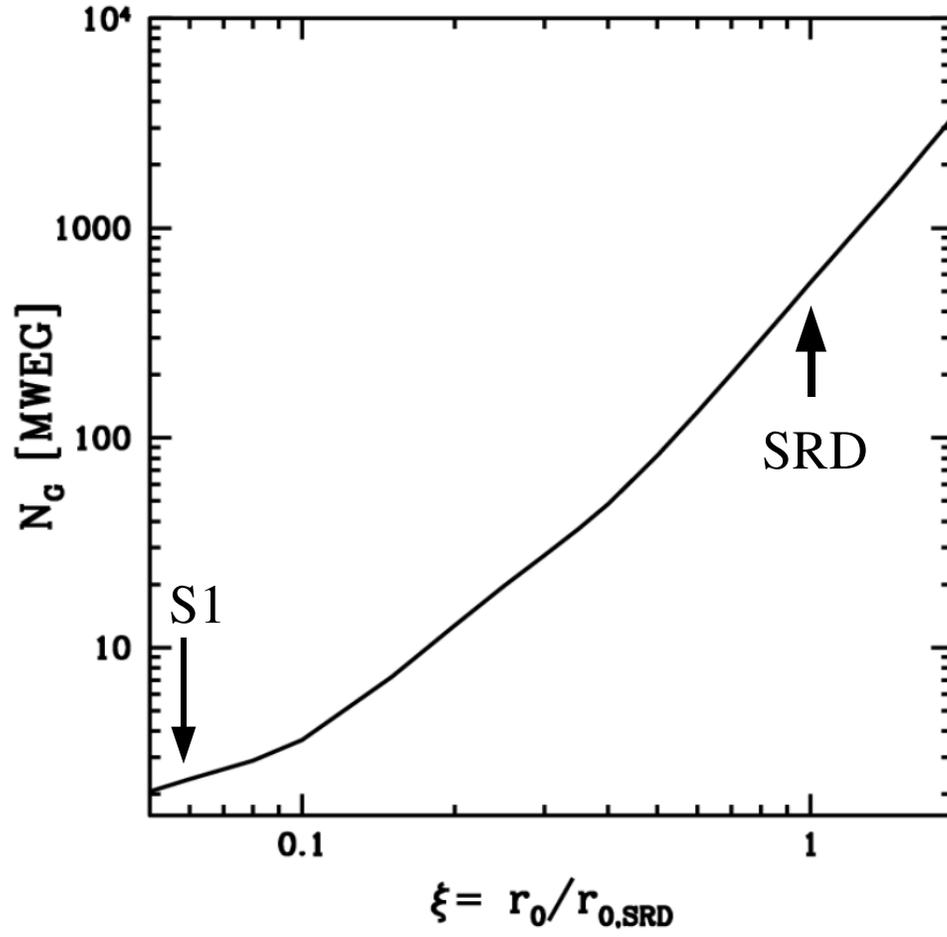


Fig. 12.— The effective number of Milky Way equivalent galaxies surveyed by LIGO as a function of detector sensitivity ξ normalized to the initial LIGO design sensitivity for NS-NS binaries. The arrow on the left denotes the instrument sensitivity achieved during the first Science Run.